Published in final edited form as:
Acta Biomater. 2014 May ; 10(5): 1836–1846. doi:10.1016/j.actbio.2013.12.005.

3D Printed Trileaflet Valve Conduits Using Biological Hydrogels and Human Valve Interstitial Cells

Bin Duan[1], **Edi Kapetanovic**[2], **Laura A. Hockaday**[1], and **Jonathan T. Butcher**[1,*]
[1]Department of Biomedical Engineering, Cornell University, Ithaca, NY, USA
[2]College of Human Ecology, Cornell University, Ithaca, NY, USA

Abstract

Tissue engineering has great potential to provide a functional de novo living valve replacement capable of integration with host tissue and growth. Among various valve conduit fabrication techniques, 3D bioprinting enables deposition of cells and hydrogels into 3D constructs with anatomical geometry and heterogeneous mechanical properties. Successful translation of this approach is however constrained by the dearth of printable and biocompatible hydrogel materials. Furthermore, it is not known how human valve cells respond to these printed environments. In this study, we develop 3D printable formulations of hybrid hydrogels based on methacrylated hyaluronic acid (Me-HA) and methacrylated gelatin (Me-Gel), and utilize them to bioprint heart valve conduits containing encapsulated human aortic valvular interstitial cells (HAVIC). Increasing Me-Gel concentration resulted in lower stiffness and higher viscosity, facilitated cell spreading, and better maintained HAVIC fibroblastic phenotype. Bioprinting accuracy was dependent upon the relative concentrations of Me-Gel and Me-HA, but when optimized enabled the fabrication of a trileaflet valve shape accurate to the original design. HAVIC encapsulated within bioprinted heart valves maintained high viability, and remodeled the initial matrix by depositing collagen and glyosaminoglycans. These findings represent the first rational design of bioprinted trileaflet valve hydrogels that regulate encapsulated human VIC behavior. The use of anatomically accurate living valve scaffolds through bioprinting may accelerate our understanding of physiological valve cell interactions and our progress towards de novo living valve replacements.

Keywords

tissue engineering; rapid prototyping; microenvironment; extracellular matrix; remodeling

1. Introduction

Heart valve disease is a serious and growing public health problem for which prosthetic replacement is most commonly indicated [1]. Tissue engineering is an attractive potential therapeutic strategy that delivers a living valve replacement capable of integration with host tissue and growth with the patient [2, 3]. Many synthetic biopolymers such as polyglycolic acid, poly(lactic acid-co-glycolic acid), and polyhydroxyalkanoates have been widely used

*Corresponding author: Department of Biomedical Engineering, Cornell University, Ithaca, NY, USA, jtb47@cornell.edu.

as fibrous or foam scaffolds for tissue engineered heart valve (TEHV) [4–7]. However, while these scaffolds provide critical initial strength for in vivo implantation, the materials are too stiff for proper valve leaflet kinematics, resulting in elevated transvalvular gradients [8]. Valve interstitial cells (VIC), the major cell population residing within the valve leaflets, respond to their local tissue stress environment by altering cellular stiffness and phenotype [9, 10]. When cultured within matrices with elevated stiffness, VIC may increase myofibroblastic characteristics that could contribute to, rather than ameliorate pathology [11, 12]. Recently, leaflet scaffolds that better mimic native properties have been fabricated by implementation of electrospinning and microfabrication techniques using synthetic polymers such as poly(ester urethane) urea (PEUU) and polyglycerol sebacate (PGS) that offer tunable and flexible mechanical and degradation properties [13–15]. But these electrospun and microfabricated membranes may be too compliant to serve as valve root and thus cannot yet be formed into complete valved conduits. These approaches are also limited in their ability to generate both anatomical complexity and heterogeneous tissue biomechanics. Hydrogels are also promising scaffold materials for tissue engineered heart valves due to their high physicochemical and mechanical tunability [16, 17], and permeability to nutrients and waste for encapsulated cells [18, 19]. In addition, hydrogels can mimic key aspects of the extracellular matrix (ECM) microenvironment to stimulate VIC function and to promote the remodeling of engineered valve constructs.

A popular method to fabricate valved conduits utilizes valvular shaped mold, within which polymer or hydrogel scaffolds (sometimes encapsulated with cells) are cast, removed, subsequently cultured [19–21]. Anatomical mold designs for heart valves are very challenging to create, forcing most researchers to use a simplified symmetric approximation that may not ultimately generate the correct mechanical and fluid dynamic environment best for the resident cells [22, 23]. Furthermore, the solution cast within the mold is necessarily homogeneous, limiting the ability to fabricate structures with internal material differences similar to the native valve [20, 24]. 3D bioprinting is an attractive extrusion based rapid prototyping (RP) technique, which can follow computer-assisted design and/or computer-assisted manufacturing design to build a complex tissue construct like a heart valve. Unlike other RP techniques (e.g., stereolithography and selective laser sintering), 3D bioprinting can incorporate biological and cellular components [25], and to introduce mechanical heterogeneity by using multiple cell types, biohybrid materials with different mechanical properties for organ or tissue printing [26, 27]. However, most bioprinting studies have utilized bioinert hydrogels like alginate, Pluronic F127, poly(ethylene glycol) dimethacrylate (PEGDMA) [25, 28, 29]. These hydrogels by themselves are poorly degradable and incompletely remodelable, both of which are important characteristics for tissue engineering applications. Other bioactive hydrogels like gelatin and hyaluronic acid are either lack of printability due to utilizing low concentration and low viscosity [30, 31], or need non-bioactive or non-biodegradable viscosity modifier like alginate and dextran [32, 33].

In this study, we generated photocrosslinkable hydrogels consisting of methacrylated hyaluronic acid (Me-HA) and methacrylated gelatin (Me-Gel) and encapsulated VIC within the hybrid hydrogels for 3D bioprinting. Hydrogel properties were tunable by varying the concentration of Me-HA and Me-Gel, which in turn changed the behavior of encapsulated VIC, including cell spreading, proliferation, glycosaminoglycan secretion and phenotype. We then implemented 3D bioprinting to fabricate a tissue engineered heart valve conduit with living leaflets based on the hybrid hydrogels.

2. Materials and Methods

2.1 Methacrylation of HA and gelatin

Me-HA (Novozymes, ~1200 kDa) was synthesized by a modification of a previously published preparation [30, 34, 35]. Briefly, 10 ml methacrylic anhydride (MA, Sigma) was reacted with HA aqueous solution at 40 °C for 6 h and the pH of mixture during reaction was maintained at 8.5 by adding 5N NaOH. Me-Gel was synthesized as previously described [30, 36]. Briefly, gelatin from bovine skin (Sigma) was dissolved at 10% (w/v) into distilled water at 40 °C and then MA (1:5 v/v to gelatin solution) was added drop by drop under stirred conditions at 40 °C for 1 h. The obtained Me-HA or Me-Gel solutions were dialyzed for 3 days and lyophilized.

2.2 Hydrogel preparation and characterization

Me-HA (2%, 4% or 6% w/v) and Me-Gel (6%, 10% or 12% w/v) were dissolved in cell culture medium with 0.05% w/v 2-hydroxy-1(4-(hydroxyethox)pheny)-2-methyl-1-propanone (Irgacure 2959; CIBA Chemicals). The gel precursor was transferred into silicon molds (Ø8 mm×1mm) and subsequently exposed to 365 nm UV light (EN-280L, Spectroline, 2.0 mW/cm^2) for 5 min. The fabricated hydrogels using Me-HA and Me-Gel with different concentration were denoted as 2% (4% or 6%) Me-HA/6% (10% or 12%) Me-Gel

Uniaxial compressive test of different hydrogels (8 mm in diameter, 2 mm in thickness, n=5) were performed using an ELF 3200 (EnduraTec) mechanical test-frame. A 250 g load cell (Sensotec) was attached to the bottom plate and a displacement sensor to the top plate with the cross-head speed of 0.075 mm/s. The displacement and load data were converted to strain and stress, respectively, by normalizing to sample thickness and area. The bulk compressive moduli were calculated from the slope of the initial linear region (5%–10% strain for compressive test) of the respective stress-strain curves. Rheological measurements were taken on an AR2000 Rheometer (TA Instruments) fitted with cone-plate geometry (cone diameter of 80 mm with a 4° angle). Stress viscosity measurements were conducted by logarithmically ramping an applied shear stress from1 to 1000 Pa at room temperature.

2.3 Cell isolation and cell culture

Human aortic VIC (HAVIC) were isolated from the aortic valve leaflets of the donor heart from 12-year old young patient undergoing cardiac transplant for a myocardial contractility mutation that is not present in valves [37]. The valve leaflets were inspected to contain no calcific deposits or thickened lesions. Tissue was procured with consent as approved by the Institutional Review Board of Weill-Cornell Medical College in New York City. Cells were cultured in MCDB131 medium (Sigma) supplemented with 10% fetal bovine serum (FBS; Invitrogen), 1% penicillin/streptomycin (P/S; Invitrogen), 0.25 μg/L recombinant human fibroblast growth factor basic (rhFGF-2; Invitrogen) and 5 μg/L recombinant human epidermal growth factor (rhEGF; Invitrogen). Cells were used at passages 4–8 [38].

For HAVIC encapsulation, monolayers of cells were trypsinized (trypsin/EDTA solution, Gibco), centrifuged and then resuspended in the hybrid hydrogels with 4% w/v Me-HA and Me-Gel with different concentration (in culture medium with Irgacure at concentration described previously) at the density of 5×10^6 cells/ml. The cell encapsulated gel was extruded into disc molds and subject to photopolymerization with UV light for 5 min. The cell-hydrogel hydrogel discs were washed with PBS and maintained at 37 °C and 5% CO_2. The medium was changed after 24 h culture and then refreshed every two days.

2.4 Cell viability, proliferation and glycosaminoglycan (GAG) secretion

The viability and circularity of encapsulated cells was determined using Live/Dead (Invitrogen) as previously described [39] and fluorescence images were obtained using a confocal laser scanning microscopy (CLSM, LSM 710, Carl Zeiss). The cell proliferation were determined using 3-(4,5-dimethylthiazol-2-yl)-2,5-diphenyltetrazolium bromide (MTT) assay [40]. Dimethylmethylene blue (DMMB) assay was performed to measure the sulfated GAG production in the hydrogels after 3 and 7 day culture [41, 42]. The constructs (n=4–5) were digested with 300 μg/ml papain in 50 mM phosphate buffer (pH 6.5), containing 5 mM cysteine and 5 mM EDTA for 16 h at 60 °C. GAG concentration was calculated by calibrating against a standard curve obtained with shark chondroitin sulfate (Sigma). To assess the biosynthetic activity of the cells, results of GAG were expressed as the ratio of GAG amount to DNA amount, which was assessed via the PicoGreen double strand DNA assay (Invitrogen).

2.5 RNA isolation and quantitative real time polymerase chain reaction (PCR)

Total RNA was extracted from cell-laden hydrogels using QIA-Shredder and RNeasy mini-kits (QIAgen) according to the manufactures' instructions. Thirty nanograms of total RNA was synthesized into first strand cDNA in a 20 μL reaction using iScript cDNA synthesis kit (BioRad Laboratories). Real-time PCR analysis was performed in a CFX Connect Real-Time PCR detection system (Bio-Rad) using SsoAdvanced SYBR Green Supermix (Bio-Rad). cDNA samples (1 μl for total volume of 20 μl per reaction) were analyzed for gene of interest and for the housekeeping gene 18S rRNA. The level of expression of each target gene was calculated using comparative Ct method (also known $2^{-\Delta\Delta Ct}$ method).

2.6 Bioprinting of 3D constructs

The Fab@Home™ open-source, open-architecture RP platform (www.fab@home.org) was used for printing the Me-HA/Me-Gel gels. Two types of 3D geometries were designed and printed. First, a cuboid shaped design with dimension of 5 mm×5 mm×1.5 mm (L×W×H) was used to evaluate the printability and printing accuracy of Me-HA/Me-Gel gels with different Me-Gel concentration. The printed constructs were imaged and the printing accuracy was assessed by comparing the measured area to the design value. The other 3D geometry we printed is a simplified heart valve structure with root and three leaflets. Both geometries are designed by Solidworks® and saved as STL files which are further imported into the printer. The software then converts the imported STL file into print paths by slicing them into layers and generating contour and fill-paths for each layer based on specific print parameters [43]. The Me-HA/Me-Gel hydrogels were loaded into the deposition syringes and extruded along the X–Y target paths for each layer. After one layer completed the print stage in was translated Z, thus sequentially building the constructs. One syringe was used to print cuboid shaped constructs. For heart valve printing, dual syringes were applied. The heart valve root was printed with acellular hydrogel, while the leaflet was printed with the Me-HA/Me-Gel hydrogels suspended with HAVIC. After printing, the cuboid shaped constructs were exposed to UV light for 5 min, while the printed heart valve conduit was subjected to four minutes photocrosslink from the top and another four minutes from the bottom.

2.7 Histology and immunohistochemistry

After 1 week culture, the bioprinted constructs were fixed, paraffin embedded, sectioned (10 μm) and stained for negatively charged GAGs using Safranin-O/fast green or for collagen using Masson's Trichrome and slides were imaged under Zeiss Discovery v20 stereo microscope (Spectra Services, Inc.)

For immunohistochemical staining, fixed laden hydrogels or sectioned bioprinted constructed were permeabilized in 0.2% Trion X-100 for 10 min at room temperature, and blocked with 1% bovine serum albumin (BSA) overnight at 4 °C. Hydrogels were treated with primary antibodies to vimentin (1:100, mouse monoclonal anti-vimentin, Invitrogen) and monoclonal anti-α-smooth muscle actin (αSMA)-Cy3 antibody (1:200, Sigma) overnight at 4 °C. Secondary fluorescent antibodies and nuclear counterstaining (via Draq 5, 1: 1000, Biostatus) were performed for 30 minutes at room temperature and then samples were imaged with Zeiss 710 CLSM.

2.8 Statistical analysis

All quantitative data are expressed as the mean±standard deviation (SD). Statistical analysis was performed using ANOVA with Scheffé post-hoc tests. A value of $p<0.05$ was considered to be statistically significant.

3. Results

3.1 Me-HA/Me-Gel hydrogel preparation and characterization

Photocrosslinkable hybrid hydrogels consisting of Me-HA and Me-Gel were first prepared in the presence of Irgacure. Me-HA and Me-Gel were synthesized by methacrylation of hydroxyl groups and primary amine groups, respectively, using methacrylic anhydride. The successful derivation was verified by ^{1}H NMR (Supplementary Figure S1). The degree of methacrylation was approximately estimated to be 22.5% for Me-HA and 61.1% for Me-Gel based on the ^{1}H NMR spectroscopy. Bulk compressive properties of Me-HA/Me-Gel hybrid hydrogels were investigated and moduli for the hydrogels with various concentrations are shown in Fig. 1A. Unexpectedly, the compressive modulus of Me-HA/Me-Gel decreased with increasing Me-Gel concentration (Fig. 1A). Me-HA/6% Me-Gel hydrogels were significantly stiffer compared to Me-HA/12% Me-Gel hydrogels ($p<0.01$). When Me-Gel concentration was fixed to be 6%, the compressive properties significantly increased with increasing Me-HA concentration from 2% to 4% and 6% ($p<0.01$). However, no significant difference was detected between hydrogels with 10% and 12% Me-Gel composition. 4% Me-HA/6% Me-Gel hydrogels with moderate Me-HA concentration and lowest Me-Gel concentration showed highest stiffness (13.0±3.2 kPa), while 6% Me-HA/12% Me-Gel hydrogels with highest viscosity at room temperature presented lowest stiffness (4.2±0.8 kPa).

We then determined hydrogel viscosity as a function of shear stress for Me-HA/Me-Gel hybrid macromers with various concentrations, as shown in Fig. 1B. For all samples, a viscosity plateau is observed at low shear stress. Generally, the zero shear viscosity of hydrogel precursors increased with increasing the concentration of Me-HA and Me-Gel. Shear thinning behavior was determined in each formulation, characterized by a decrease in viscosity with increased shear stress. The wall shear stress that occurs in our 3D printer ranges from around 100 Pa to 800 Pa [44], as indicated by dash line in Fig. 1B. Within this shear stress range, the hybrid hydrogel precursors with 2% Me-HA and 6–10% Me-Gel showed viscosity value lower than 100 Pa·S, which is too watery to hold the printed shape. On the contrary, Me-HA/Me-Gel hydrogels with 6% Me-HA and 10–12% Me-Gel with viscosity more than 10^4 Pa·S are too viscous and difficult to be deposited smoothly. Therefore, we used the hybrid hydrogels with 4% Me-HA and 6%, 10% and 12% Me-Gel for follow-on investigations of encapsulated HAVIC behavior and bioprinting.

3.2 HAVIC viability, morphology, proliferation and GAG deposition within hydrogels

Fig. 2 presents cell viability and cell circularity measured based on Live/Dead images obtained at least 50 μm below the hydrogel surface in order to avoid any interference from

spread cells attached on the hydrogel surface. The near exclusive green fluorescence in Fig. 2A shows that the encapsulated VIC in Me-HA/Me-Gel hydrogels with various Me-Gel concentrations were almost all alive after 3 day and 7 day culture. Cell viability was higher than 90% for all the hydrogel conditions (Fig.2B). Most encapsulated VIC remained spherical in shape after 3 days culture and more cells had spreading morphology within the hydrogels on day 7, showing significantly lower cell circularity with increasing the culture time (Fig. 2C). On day 3, the circularity for VIC in 4%Me-HA/12%Me-Gel hydrogels with lower stiffness was significantly lower than that in 4%Me-HA/6%Me-Gel hydrogels with higher stiffness, as shown in Fig. 2C. Similarly, after 7 day culture, the stiffer hybrid hydrogels (4%Me-HA/6%Me-Gel and 4%Me-HA/10%Me-Gel) delayed cell spreading and exhibited significantly higher cell circularity comparing to softer hydrogels (4%Me-HA/12%Me-Gel).

MTT assay was also used to quantify the cellular metabolic activity of encapsulated HAVIC within the 3D hydrogels. As shown in Fig. 3A, HAVIC in all the hydrogels proliferated during 7 day culture, with significant increase in MTT absorbance comparing to day 3 ($p<0.01$). During the first 3 day culture, the MTT absorption for stiffer hydrogels (4%Me-HA/6%Me-Gel) was significantly higher than that of softer hydrogels (4%Me-HA/12%Me-Gel). However, there was no significant difference in proliferation rate for different Me-HA/Me-Gel hydrogel formulations at day 7.

The level of sulfated GAG produced by encapsulated VIC in different hydrogels after 3 and 7 day culture was quantitatively determined by modified DMMB assay. The GAG content of Me-HA/Me-Gel hybrid hydrogels was measured to be markedly higher on day 7 comparing to day 3 ($p<0.01$), as shown in Fig. 3B. On day 3, the GAG/DNA value was significantly higher for 4%Me-HA/12%Me-Gel than 4%Me-HA/6%Me-Gel ($p<0.01$). However, on day 7, no significant difference of GAG content was detected for different hydrogel samples. This may be because that HAVIC remodel the hydrogels by secreting different matrix components at different times/rates.

3.3 HAVIC phenotypes and gene expression

As shown in Fig. 4, the encapsulated HAVIC expressed both αSMA and vimentin within all the hydrogel samples after 7 day culture, indicating the activation of HAVIC from fibroblastic to myofibroblastic phenotype. Quantitative analysis of gene expression was conducted using real-time PCR, normalized to 18S, and expressed relative to 4%Me-HA/6%Me-Gel. On both day 3 and day 7, 4%Me-HA/6%Me-Gel expressed less αSMA vimentin and periostin than 4%Me-HA/10%Me-Gel and 4%Me-HA/12%Me-Gel hydrogels with lower stiffness ($p<0.01$) (Fig. 5A B and C). As shown in Fig. 5B, vimentin gene expression was dramatically increased with decreasing stiffness of different hydrogels ($p<0.01$). No significant difference was observed among the hydrogels for collagen I expression (Fig. 5D). With increasing the culture time, expression of αSMA was significantly upregulated for 4%Me-HA/6%Me-Gel. In addition, periostin and collagen I expression was significantly elevated for all the hydrogels after 7 day culture comparing to day 3 (for periostin, $p<0.05$ for 4%Me-HA/6%Me-Gel and $p<0.01$ for 4%Me-HA/10%Me-Gel and 4%Me-HA/12%Me-Gel; for collagen I, $p<0.05$).

3.4 Bioprinting of 3D constructs

A simple cuboid shaped constructs were first printed using the hybrid hydrogels with different Me-Gel concentration, as shown in Fig. 6. The hydrogels with lower viscosity (4%Me-HA/6%Me-Gel and 4%Me-HA/10%Me-Gel) better maintained their geometry and mechanical integrity after extrusion and crosslinking (Fig. 6A, B), while the printed constructs using 4%Me-HA/12%Me-Gel had incomplete and missing structure (Fig. 6C).

The printing accuracy (percentage overlap of printed to designed area) for 4%Me-HA/6%Me-Gel and 4%Me-HA/10%Me-Gel was 124.0±11.6% and 111.3±7.2%, respectively, which indicated that the constructs spread after printing and had larger area than design. In contrast, 4%Me-HA/12%Me-Gel printed constructs had smaller area and lower printing accuracy (74.9±5.4%). In all the printed constructs, high HAVIC viability (>90%) was observed for the cells encapsulated to depths exceeding 700 μm below the surface (Supplementary Figure S2). This indicated that the printed constructs could be fed completely via nutrient diffusion.

We thus implemented 4%Me-HA/10%Me-Gel hydrogels for further bioprinting of heart valve conduits by considering hydrogel properties, encapsulated cell behavior, and bioprinting accuracy. A simplified trileaflet heart valve model was designed by Solidwork®, as shown in Fig. 7A. The model has inner diameter of 20 mm, outer diameter of 26 mm and height of 8 mm for valve root, and three leaflets with radius of 10 mm. The heart valve conduits were successfully bioprinted with acellular root and HAVIC encapsulated leaflets using 4%Me-HA/10%Me-Gel hydrogels (Fig. 7B). The bioprinted valve conduits well maintained the structure after photocrosslink and static culture for 7 days (Fig. 7C). As shown in Fig. 7D, nearly all encapsulated cells (92.1±2.5%) were alive, even for the cells that were several hundred micrometers below the surface, indicating the capacity of oxygen, nutrition supply and waste removal. In addition, HAVIC were found to be subconfluent on the conduit surface. Fig. 7E and F shows the histological staining of encapsulated HAVIC within printed Me-HA/Me-Gel conduits. Although negatively charged Me-HA attracted the cationic Safranin O dye and showed pink color, the encapsulated individual cells were observed to be surrounded by an ECM containing sulfated GAG, as indicated by Safranin O staining (Fig. 7E). Similar observations were also reported in valve conduits by other researchers [45, 46]. The sulfated GAG content of printed leaflets was measured to be 61.3±9.5 μg GAG/μg DNA, which was less than that of 4%Me-HA/10%Me-Gel hydrogel discs. Masson's Trichrome staining of printed leaflets showed that more intense blue color was found around the encapsulated HAVIC, indicating the newly deposition of collagen (Fig. 7F). The encapsulated HAVIC also expressed both αSMA and vimentin protein after 7 days culture.

4. Discussion

3D bioprinting is a versatile technique that has great potential to fabricate heterogeneous tissues with multiple cell types and biohybrid materials with different mechanical properties [39, 47, 48]. However, there is a pressing need to develop more enabling bioactive, biofunctional materials for 3D bioprinting, and to understand how printed microenvironmental features affect encapsulated cell phenotype [49]. We describe here the 3D bioprinting of living heart valve conduits based on photocrosslinkable Me-HA and Me-Gel hybrid hydrogels. The major objectives of this study were to: 1) identify the range of hybrid hydrogel composition for bioprinting, and 2) to determine how encapsulated HAVIC are altered within this range and the effects of printable microenvironment on HAVIC behavior.

The bioprinted materials, material processing and environmental conditions (UV exposure, temperature, *et al.*) should ensure encapsulated cell viability and phenotypes. Different from many printable bioinert materials like alginate, agarose, Pluronic F127, *et al*., HA and gelatin are well-known bioactive biomaterials with cell adhesion and cell degradation motifs. Me-HA and Me-Gel are also widely used for various cell encapsulations [36, 50, 51]. Recently, Me-HA/Me-Gel hybrid hydrogels has been reported to support human umbilical cord vein endothelial cells [52] and regulate valve interstitial cell behavior [30]. Skardal *et al.* has also implemented Me-HA/Me-Gel hybrid hydrogels for bioprinting of

simple cylindrical tissue constructs, but the required pre-crosslinked materials limit the size and/or accuracy of printable geometries [31, 44]. In this study, we first characterized the mechanical properties and viscosity of different Me-HA/Me-Gel hybrid hydrogels, which potentially can be used for bioprinting. The compressive properties of hybrid hydrogels are tunable by varying the component concentrations. Unexpectedly, the compressive properties were not enhanced by increasing polymer concentration, which was in contrast to previous studies reported by other researchers [52, 53]. This is probably because relatively high viscosity of the hybrid hydrogels investigated in this study results in lower photocrosslink efficiency and density which are known to greatly affect mechanical properties of hydrogels [54, 55]. When Me-HA concentration was fixed, increasing Me-Gel concentration further increases the viscosity due to the concentration and the thermoreversible gelation effect, and thus significantly decreases the compressive properties of hybrid hydrogels. However, the viscosity and stiffness were independent of each other when considering both Me-HA and Me-Gel concentrations (Supplementary Figure S3). These levels of stiffness are within the range of local and global elastic moduli of VIC (~3–20 kPa) cultured on polyacrylamide substrates with different stiffness (3–144 kPa) [56]. Most TEHV research has focused on replicating the material stiffness at failure strain [57–59], which is much stiffer than in vivo physiological stiffness and very rarely encountered by resident cells during physiological function [60]. These highlight the need to identify and replicate the physiological biomechanical targets of the heart valve in TEHV biomaterial design. The Me-HA/Me-Gel hybrid hydrogels may thus better mimic the leaflets with the mechanical properties in the physiological strain range.

Bioprintable materials need enough fluidity to be extruded intact through a narrow tube/needle, but yet retain sufficient viscosity to hold shape after printing and before crosslinking [25]. The viscosity of Me-HA/Me-Gel hybrid hydrogels is dependent on the applied sheer stress. Within the shear stress range that works during extrusion process, the hybrid hydrogels with 2% Me-HA are less viscous to hold the printed shape, whereas 6% Me-HA hydrogels are too viscous to be smoothly deposited. The mostly suitable hydrogel viscosity range for Fab@Home 3D bioprinting system in this study is from around 400 to 4000 Pa·s. The suspended cells probably reside in the middle of the tip and are protected from wall shear during extrusion [44]. The hybrid hydrogels with 4% Me-HA and 6%, 10% and 12% Me-Gel are thus more appropriate for 3D bioprinting. It is also of significant importance to investigate the cellular behaviors of encapsulated cells within bioprintable microenvironment. Increasing Me-Gel concentration from 6% to 12% decreased the hydrogel stiffness and increased the cell adhesion density. The change of microenvironment improved cell spreading and increased GAG secretion in 3 day culture. Cell spreading depends on the matrix stiffness and cell adhesion site density [30, 61, 62]. Increasing hydrogel stiffness decreases the pore size, which limits the space for cellular elongation, spreading, and migration [63, 64], while increase of cell adhesion site density promotes cell adhesion [65, 66] and affects subsequent cellular events like proliferation [67], migration [62], and differentiation [68, 69]. In addition, the more spreading HAVIC within hybrid Me-HA/Me-Gel hydrogels (4% Me-HA/10% Me-Gel, 4% Me-HA/12% Me-Gel) had more expression of all the target genes (αSMA, vimentin, periostin and collagen I), indicating that the encapsulated HAVIC are more active. Decreasing stiffness while increasing cell adhesion site density in Me-HA/Me-Gel hydrogels upregulated vimentin, which is one of major biomarkers of fibroblastic phenotype of VIC. This indicates addition of Me-Gel decreased myofibroblastic activation, which is consistent with our previous findings with non-printable hybrid hydrogel formulations [30]. Overall, by changing the concentration of gelatin component, Me-HA/Me-Gel hydrogels demonstrated tunable 3D microenvironments that can regulate cellular response.

By combining 3D bioprinting with optimized Me-HA/Me-Gel hybrid hydrogels, we generated trileaflet heart valve conduits with morphologically similar to the original CAD design with direct encapsulation of HAVIC within the printed leaflets. Strategies to develop anatomically accurate and mechanically heterogeneous living heart valve conduits with similar ECM microenvironment to native tissue has gained importance for the advancement of heart valve tissue engineering [70]. We previously showed that we could generate anatomically complex valves via 3D bioprinting [39, 43]. 3D bioprinting technique is also capable of fabricating full valve conduits (consisting of both valve leaflets and root). In this study, we used the model with simplified valve geometry instead of natural anatomy to test the bioprintability of the hybrid hydrogels and focused on the response of encapsulated HAVIC within bioprinted valve leaflets. One concern for hydrogel based tissue and organ printing is the cell viability and functions within the constructs [49]. In this study, the encapsulated HAVIC kept high cell viability (>90%) after extrusion during printing process and further photocrosslink. In addition, cells easily adhered to, and formed a monolayer on the bioprinted construct surface, while the encapsulated cells below the surface started to remodel the hydrogel after 3 day culture. Successful tissue engineered heart valve strategies must enable cells to remodel their initial microenvironment and secret their own ECM [71, 72]. The Me-HA/Me-Gel hydrogels we developed were remodeled by the HAVIC. Since these components are ECM analogs, excellent biodegradability and bioactivity can be expected as previously shown [73, 74].

Apart from cell viability, there are several other key challenges for tissue and organ printing, including (1) the resolution of bioprinter and accuracy of bioprinted constructs; (2) vascularization; (3) heterogeneous structure and biomechanics. Fab@Home 3D bioprinting platform supports fabrication of tissue constructs with anatomical shape [43] and potentially enables heterogeneous printing of tissue constructs using multiple materials and cell types [26, 39]. Systematic optimization of printing conditions and parameters can improve the accuracy of 3D printing platforms for biofabrication and tissue engineering applications [44, 75]. Healthy human valve leaflets are almost entirely avascular [1, 76] and this structure only requires diffusion of nutrients and metabolites. The 3D cell-laden hydrogel construct with reasonable thickness can fulfill this requirement and thus maintain high cell viability and normal phenotype for valve cells. The bioprinted hydrogel based valve conduits also provide more suitable physiological environment to VIC comparing to other synthetic polymers which have much higher stiffness and may pathologically active myofibroblastic phenotype of VIC [9, 77]. The short-term static culture of our printed constructs represents a first step towards creating a mature, functional valve conduit. These printed hydrogel valve constructs do not yet fulfill the full mechanical range of native valve tissue, though we believe that fidelity of the physiological domain of biomechanical performance is as important as its failure material strength characteristics. Further enhancement of material properties of bioprinted valve conduits can be achieved through conditioning in pulsatile bioreactor, as has been demonstrated with many other groups [78, 79]. It is not yet clear how hemodynamic stimulation affects the shape change and remodeling of printed valve conduits. Through the 3D printing approach, we can in the future address how important prescribed material composition and its spatial organization contribute to macro and micro-scale valve structural and mechanical fidelity.

5. Conclusions

This study has demonstrated 3D bioprinting of living heart valve conduits based on photocrosslinkable Me-HA/Me-Gel hydrogels with tunable physical properties. The hybrid hydrogels can well support the encapsulated HAVIC and regulate cellular response by varying hybrid hydrogel composition. Increasing Me-Gel concentration resulted in hydrogel stiffness decrease and cell adhesion density increase and thus facilitated HAVIC spreading

morphology and better maintained fibroblastic phenotypes of HAVIC. By implementing 3D bioprinting technique and Me-HA/Me-Gel hydrogels with optimized composition and properties, we generated living trileaflet heart valve conduit with decent accuracy, high cell viability and remodeling potential. Our findings herein expand the library of biomaterials which can be utilized for 3D bioprinting, and provide important insight into the design of bioprintable microenvironment for regulating VIC behavior. 3D bioprinted valve conduits are thus a promising strategy for tissue engineered living valve replacements and are also encouraging in vitro models toward improving valve scaffold designs and investigating valve disease mechanisms.

Supplementary Material

Refer to Web version on PubMed Central for supplementary material.

Acknowledgments

This work was funded by the American Heart Association Postdoctoral Fellowship (13POST17220071), Morgan Family Foundation, The Hartwell Foundation, the National Science Foundation (CBET-0955172) NSF Graduate Research Fellowship, Fondation LeDucq MITRAL Transnational Network, and the National Institutes of Health (HL110328, HL118672). We thank Dr. Jonathan Chen in the Department of Cardiothoracic Surgery at Weill Cornell Medical College for providing human aortic valve tissue. We would like to thank Microscopy and Imaging Facility, Life Sciences Core Laboratories Center in Cornell University for their assistance with CLSM imaging. The authors have no financial disclosures.

References

1. Butcher JT, Mahler GJ, Hockaday LA. Aortic valve disease and treatment: The need for naturally engineered solutions. Adv Drug Deliv Rev. 2011; 63:242–268. [PubMed: 21281685]
2. Mendelson K, Schoen FJ. Heart valve tissue engineering: Concepts, approaches, progress, and challenges. Ann Biomed Eng. 2006; 34:1799–1819. [PubMed: 17053986]
3. Filova E, Straka F, Mirejovsky T, Masin J, Bacakova L. Tissue-engineered heart valves. Physiol Res. 2009; 58:S141–S158. [PubMed: 20131932]
4. Shum-Tim D, Stock U, Hrkach J, Shinoka T, Lien J, Moses MA, Stamp A, Taylor G, Moran AM, Landis W, Langer R, Vacanti JP, Mayer JE. Tissue engineering of autologous aorta using a new biodegradable polymer. Ann Thorac Surg. 1999; 68:2298–2304. [PubMed: 10617020]
5. Hoerstrup SP, Sodian R, Daebritz S, Wang J, Bacha EA, Martin DP. Functional living trileaflet heart valves grown in vitro. Circulation. 2000; 102:III44–49. [PubMed: 11082361]
6. Hoerstrup SP, Kadner A, Melnitchouk S, Trojan A, Eid K, Tracy J, Sodian R, Visjager JF, Kolb S, Grunenfelder J, Zund G, Turina MI. Tissue engineering of functional trileaflet heart valves from human marrow stromal cells. Circulation. 2002; 106:I143–I150. [PubMed: 12354724]
7. Schmidt D, Dijkman PE, Driessen-Mol A, Stenger R, Mariani C, Puolakka A, Rissanen M, Deichmann T, Odermatt B, Weber B, Emmert MY, Zund G, Baaijens FPT, Hoerstrup SP. Minimally-invasive implantation of living tissue engineered heart valves A comprehensive approach from autologous vascular cells to stem cells. J Am Coll Cardiol Cardiology. 2010; 56:510–520.
8. Merryman WD, Youn I, Lukoff HD, Krueger PM, Guilak F, Hopkins RA, Sacks MS. Correlation between heart valve interstitial cell stiffness and transvalvular pressure: implications for collagen biosynthesis. Am J Physiol-Heart Circul Physiol. 2006; 290:H224–H231.
9. Kloxin AM, Benton JA, Anseth KS. In situ elasticity modulation with dynamic substrates to direct cell phenotype. Biomaterials. 2010; 31:1–8. [PubMed: 19788947]
10. Wyss K, Yip CYY, Mirzaei Z, Jin XF, Chen JH, Simmons CA. The elastic properties of valve interstitial cells undergoing pathological differentiation. J Biomech. 2012; 45:882–887. [PubMed: 22189247]

11. Schmidt D, Mol A, Odermatt B, Neuenschwander S, Breymann C, Gossi M, Genoni M, Zund G, Hoerstrup SP. Engineering of biologically active living heart valve leaflets using human umbilical cord-derived progenitor cells. Tissue Eng. 2006; 12:3223–3232. [PubMed: 17518636]
12. Kadner A, Hoerstrup SP, Zund G, Eid K, Maurus C, Melnitchouk S, Grunenfelder J, Turina MI. A new source for cardiovascular tissue engineering: human bone marrow stromal cells. Eur J Cardio-Thorac Surg. 2002; 21:1055–1060.
13. Sant S, Iyer D, Gaharwar AK, Patel A, Khademhosseini A. Effect of biodegradation and de novo matrix synthesis on the mechanical properties of valvular interstitial cell-seeded polyglycerol sebacate-polycaprolactone scaffolds. Acta Biomater. 2013; 9:5963–5973. [PubMed: 23168222]
14. Amoroso NJ, D'Amore A, Hong Y, Rivera CP, Sacks MS, Wagner WR. Microstructural manipulation of electrospun scaffolds for specific bending stiffness for heart valve tissue engineering. Acta Biomater. 2012; 8:4268–4277. [PubMed: 22890285]
15. Masoumi N, Johnson KL, Howell MC, Engelmayr GC. Valvular interstitial cell seeded poly(glycerol sebacate) scaffolds: Toward a biomimetic in vitro model for heart valve tissue engineering. Acta Biomater. 2013; 9:5974–5988. [PubMed: 23295404]
16. Jia XQ, Kiick KL. Hybrid multicomponent hydrogels for tissue engineering. Macromol Biosci. 2009; 9:140–156. [PubMed: 19107720]
17. Kloxin AM, Kloxin CJ, Bowman CN, Anseth KS. Mechanical properties of cellularly responsive hydrogels and their experimental determination. Adv Mater. 2010; 22:3484–3494. [PubMed: 20473984]
18. Flanagan TC, Wilkins B, Black A, Jockenhoevel S, Smith TJ. A collagen-glycosaminoglycan co-culture model for heart valve tissue engineering applications. Biomaterials. 2006; 27:2233–2246. [PubMed: 16313955]
19. Flanagan TC, Cornelissen C, Koch S, Tschoeke B, Sachweh JS, Schmitz-Rode T, Jockenhoevel S. The in vitro development of autologous fibrin-based tissue-engineered heart valves through optimised dynamic conditioning. Biomaterials. 2007; 28:3388–3397. [PubMed: 17467792]
20. Tedder ME, Simionescu A, Chen J, Liao J, Simionescu DT. Assembly and testing of stem cell-seeded layered collagen constructs for heart valve tissue engineering. Tissue Eng Part A. 2011; 17:25–36. [PubMed: 20673028]
21. Sacks MS, Schoen FJ, Mayer JEJ. Bioengineering challenges for heart valve tissue engineering. Annu Rev Biomed Eng. 2009; 11:289–313. [PubMed: 19413511]
22. Syedain ZH, Tranquillo RT. Controlled cyclic stretch bioreactor for tissue-engineered heart valves. Biomaterials. 2009; 30:4078–4084. [PubMed: 19473698]
23. Weber M, Heta E, Moreira R, Gesché V, Schermer T, Frese J, Jockenhoevel S, Mela P. Tissue-engineered fibrin-based heart valve with a tubular leaflet design. Tissue Eng Part C. 201310.1089/ten.TEC.2013.0258
24. Albanna MZ, Bou-Akl TH, Walters HL, Matthew HWT. Improving the mechanical properties of chitosan-based heart valve scaffolds using chitosan fibers. J Mech Behav Biomed Mater. 2012; 5:171–180. [PubMed: 22100092]
25. Chang CC, Boland ED, Williams SK, Hoying JB. Direct-write bioprinting three-dimensional biohybrid systems for future regenerative therapies. J Biomed Mater Res Part B. 2011; 98B:160–170.
26. Skardal A, Zhang JX, Prestwich GD. Bioprinting vessel-like constructs using hyaluronan hydrogels crosslinked with tetrahedral polyethylene glycol tetracrylates. Biomaterials. 2010; 31:6173–6181. [PubMed: 20546891]
27. Fedorovich NE, Wijnberg HM, Dhert WJA, Alblas J. Distinct tissue formation by heterogeneous printing of osteo- and endothelial progenitor cells. Tissue Eng Part A. 2011; 17:2113–2121. [PubMed: 21513466]
28. Khalil S, Sun W. Bioprinting endothelial cells with alginate for 3D tissue constructs. J Biomech Eng-Trans ASME. 2009; 131:111002.
29. Cui XF, Breitenkamp K, Finn MG, Lotz M, D'Lima DD. Direct human cartilage repair using three-dimensional bioprinting technology. Tissue Eng Part A. 2012; 18:1304–1312. [PubMed: 22394017]

30. Duan B, Hockaday LA, Kapetanovic E, Kang KH, Butcher JT. Stiffness and adhesivity control aortic valve interstitial cell behavior within hyaluronic acid based hydrogels. Acta Biomater. 2013; 9:7640–7650. [PubMed: 23648571]
31. Skardal A, Zhang JX, McCoard L, Xu XY, Oottamasathien S, Prestwich GD. Photocrosslinkable hyaluronan-gelatin hydrogels for two-step bioprinting. Tissue Eng Part A. 2010; 16:2675–2685. [PubMed: 20387987]
32. Li SJ, Xiong Z, Wang XH, Yan YN, Liu HX, Zhang RJ. Direct Fabrication of a hybrid cell/hydrogel construct by a double-nozzle assembling technology. J Bioact Compat Polym. 2009; 24:249–265.
33. Pescosolido L, Schuurman W, Malda J, Matricardi P, Alhaique F, Coviello T, van Weeren PR, Dhert WJA, Hennink WE, Vermonden T. Hyaluronic acid and dextran-based semi-IPN hydrogels as biomaterials for bioprinting. Biomacromolecules. 2011; 12:1831–1838. [PubMed: 21425854]
34. Smeds KA, Pfister-Serres AM, KDD, Inoue M, Hatchell DL, Grinstaff MW. Photocrosslinkable polysaccharides for in situ hydrogel formation. J Biomed Mater Res. 2001; 55:254–255.
35. Brigham MD, Bick A, Lo E, Bendali A, Burdick JA, Khademhosseini A. Mechanically robust and bioadhesive collagen and photocrosslinkable hyaluronic acid semi-interpenetrating networks. Tissue Eng Part A. 2009; 15:1645–1653. [PubMed: 19105604]
36. Nichol JW, Koshy ST, Bae H, Hwang CM, Yamanlar S, Khademhosseini A. Cell-laden microengineered gelatin methacrylate hydrogels. Biomaterials. 2010; 31:5536–5544. [PubMed: 20417964]
37. Richards J, El-Hamamsy I, Chen S, Sarang Z, Sarathchandra P, Yacoub MH, Chester AH, Butcher JT. Side-specific endothelial-dependent regulation of aortic valve calcification interplay of hemodynamics and nitric oxide signaling. Am J Pathol. 2013; 182:1922–1931. [PubMed: 23499458]
38. Taylor PM, Sachlos E, Dreger SA, Chester AH, Czernuszka JT, Yacoub MH. Interaction of human valve interstitial cells with collagen matrices manufactured using rapid prototyping. Biomaterials. 2006; 27:2733–2737. [PubMed: 16406000]
39. Duan B, Hockaday LA, Kang KH, Butcher JT. 3D bioprinting of heterogeneous aortic valve conduits with alginate/gelatin hydrogels. J Biomed Mater Res Part A. 2012; 101A:1255–1264.
40. Duan B, Wang M, Zhou WY, Cheung WL, Li ZY, Lu WW. Three-dimensional nanocomposite scaffolds fabricated via selective laser sintering for bone tissue engineering. Acta Biomater. 2010; 6:4495–4505. [PubMed: 20601244]
41. Farndale RW, Buttle DJ, Barrett AJ. Improved quantitation and discrimination of sulphated glycosaminoglycans by use of dimethylmethylene blue. Biochim Biophys Acta. 1986; 883:173–177. [PubMed: 3091074]
42. Hui TY, Cheung KMC, Cheung WL, Chan D, Chan BP. In vitro chondrogenic differentiation of human mesenchymal stem cells in collagen microspheres: Influence of cell seeding density and collagen concentration. Biomaterials. 2008; 29:3201–3212. [PubMed: 18462789]
43. Hockaday LA, Kang KH, Colangelo NW, Cheung PYC, Duan B, Malone E, Wu J, Girardi LN, Bonassar LJ, Lipson H, Chu CC, Butcher JT. Rapid 3D printing of anatomically accurate and mechanically heterogeneous aortic valve hydrogel scaffolds. Biofabrication. 2012; 4:035005. [PubMed: 22914604]
44. Kang KH, Hockaday LA, Butcher JT. Quantitative optimization of solid freeform deposition of aqueous hydrogels. Biofabrication. 2013; 5:035001. [PubMed: 23636927]
45. Liao E, Yaszemski M, Krebsbach P, Hollister S. Tissue-engineered cartilage constructs using composite hyaluronic acid/collagen I hydrogels and designed poly(propylene fumarate) scaffolds. Tissue Eng. 2007; 13:537–550. [PubMed: 17319795]
46. Burdick JA, Chung C, Jia XQ, Randolph MA, Langer R. Controlled degradation and mechanical behavior of photopolymerized hyaluronic acid networks. Biomacromolecules. 2005; 6:386–391. [PubMed: 15638543]
47. Xu T, Binder KW, Albanna MZ, Dice D, Zhao WX, Yoo JJ, Atala A. Hybrid printing of mechanically and biologically improved constructs for cartilage tissue engineering applications. Biofabrication. 2013; 5:015001. [PubMed: 23172542]

48. Fedorovich NE, Schuurman W, Wijnberg HM, Prins HJ, van Weeren PR, Malda J, Alblas J, Dhert WJA. Biofabrication of osteochondral tissue equivalents by printing topologically defined, cell-laden hydrogel scaffolds. Tissue Eng Part C. 2012; 18:33–44.
49. Billiet T, Vandenhaute M, Schelfhout J, Van Vlierberghe S, Dubruel P. A review of trends and limitations in hydrogel-rapid prototyping for tissue engineering. Biomaterials. 2012; 33:6020–6041. [PubMed: 22681979]
50. Chung C, Burdick JA. Influence of three-dimensional hyaluronic acid microenvironments on mesenchymal stem cell chondrogenesis. Tissue Eng Part A. 2009; 15:243–254. [PubMed: 19193129]
51. Hachet E, Van Den Berghe H, Bayma E, Block MR, Auzely-Velty R. Design of biomimetic cell-interactive substrates using hyaluronic acid hydrogels with tunable mechanical properties. Biomacromolecules. 2012; 13:1818–1827. [PubMed: 22559074]
52. Camci-Unal G, Cuttica D, Annabi N, Demarchi D, Khademhosseini A. Synthesis and characterization of hybrid hyaluronic acid-gelatin hydrogels. Biomacromolecules. 2013; 14:1085–1092. [PubMed: 23419055]
53. Hutson CB, Nichol JW, Aubin H, Bae H, Yamanlar S, Al-Haque S, Koshy ST, Khademhosseini A. Synthesis and characterization of tunable poly(ethylene glycol): Gelatin methacrylate composite hydrogels. Tissue Eng Part A. 2011; 17:1713–1723. [PubMed: 21306293]
54. Jeon O, Bouhadir KH, Mansour JM, Alsberg E. Photocrosslinked alginate hydrogels with tunable biodegradation rates and mechanical properties. Biomaterials. 2009; 30:2724–2734. [PubMed: 19201462]
55. Shi JB, Xing MM, Zhong W. Development of hydrogels and biomimetic regulators as tissue engineering scaffolds. Membranes. 2012; 2:70–90.
56. Liu H, Sun Y, Simmons CA. Determination of local and global elastic moduli of valve interstitial cells cultured on soft substrates. J Biomech. 2013; 46:1967–1971. [PubMed: 23746597]
57. Sacks MS, Merryman WD, Schmidt DE. On the biomechanics of heart valve function. J Biomech. 2009; 42:1804–1824. [PubMed: 19540499]
58. Stephens EH, Chu CK, Grande-Allen KJ. Valve proteoglycan content and glycosaminoglycan fine structure are unique to microstructure, mechanical load and age: Relevance to an age-specific tissue-engineered heart valve. Acta Biomater. 2008; 4:1148–1160. [PubMed: 18448399]
59. Robinson PS, Tranquillo RT. Planar biaxial behavior of fibrin-based tissue-engineered heart valve leaflets. Tissue Eng Part A. 2009; 15:2763–2772. [PubMed: 19368523]
60. Zhao RG, Sider KL, Simmons CA. Measurement of layer-specific mechanical properties in multilayered biomaterials by micropipette aspiration. Acta Biomater. 2011; 7:1220–1227. [PubMed: 21056128]
61. Sant S, Hancock MJ, Donnelly JP, Iyer D, Khademhosseini A. Biomimetic gradient hydrogels for tissue engineering. Can J Chem Eng. 2010; 88:899–911. [PubMed: 21874065]
62. Lei YG, Gojgini S, Lam J, Segura T. The spreading, migration and proliferation of mouse mesenchymal stem cells cultured inside hyaluronic acid hydrogels. Biomaterials. 2011; 32:39–47. [PubMed: 20933268]
63. Chen YC, Lin RZ, Qi H, Yang YZ, Bae HJ, Melero-Martin JM, Khademhosseini A. Functional human vascular network generated in photocrosslinkable gelatin methacrylate hydrogels. Adv Funct Mater. 2012; 22:2027–2039. [PubMed: 22907987]
64. Brandl F, Sommer F, Goepferich A. Rational design of hydrogels for tissue engineering: Impact of physical factors on cell behavior. Biomaterials. 2007; 28:134–146. [PubMed: 17011028]
65. Zhang Z, Lai YX, Yu L, Ding JD. Effects of immobilizing sites of RGD peptides in amphiphilic block copolymers on efficacy of cell adhesion. Biomaterials. 2010; 31:7873–7882. [PubMed: 20674012]
66. Tocce EJ, Broderick AH, Murphy KC, Liliensiek SJ, Murphy CJ, Lynn DM, Nealey PF. Functionalization of reactive polymer multilayers with RGD and an antifouling motif: RGD density provides control over human corneal epithelial cell-substrate interactions. J Biomed Mater Res Part A. 2012; 100A:84–93.
67. Jun I, Kim SJ, Choi E, Park KM, Rhim T, Park J, Park KD, Shin H. Preparation of biomimetic hydrogels with controlled cell adhesive properties and topographical features for the study of

muscle cell adhesion and proliferation. Macromol Biosci. 2012; 12:1502–1513. [PubMed: 22965817]

68. Kim IL, Khetan S, Baker BM, Chen CS, Burdick JA. Fibrous hyaluronic acid hydrogels that direct MSC chondrogenesis through mechanical and adhesive cues. Biomaterials. 2013; 34:5571–5580. [PubMed: 23623322]
69. Wang X, Yan C, Ye K, He Y, Li ZH, Ding JD. Effect of RGD nanospacing on differentiation of stem cells. Biomaterials. 2013; 34:2865–2874. [PubMed: 23357372]
70. Rippel RA, Ghanbari H, Seifalian AM. Tissue-engineered heart valve: future of cardiac surgery. World J Surg. 2012; 36:1581–1591. [PubMed: 22395345]
71. Su FC, Wu CC, Chien S. Review: Roles of microenvironment and mechanical forces in cell and tissue remodeling. J Med Biol Eng. 2011; 31:233–244.
72. Cowin SC. Tissue growth and remodeling. Annu Rev Biomed Eng. 2004; 6:77–107. [PubMed: 15255763]
73. Prestwich GD. Hyaluronic acid-based clinical biomaterials derived for cell and molecule delivery in regenerative medicine. J Control Release. 2011; 155:193–199. [PubMed: 21513749]
74. Erickson IE, Kestle SR, Zellars KH, Farrell MJ, Kim M, Burdick JA, Mauck RL. High mesenchyrnal stem cell seeding densities in hyaluronic acid hydrogels produce engineered cartilage with native tissue properties. Acta Biomater. 2012; 8:3027–3034. [PubMed: 22546516]
75. Castilho M, Pires I, Gouveia B, Rodrigues J. Structural evaluation of scaffolds prototypes produced by three-dimensional printing. Int J Adv Manuf Tech. 2011; 56:561–569.
76. Soini Y, Salo T, Satta J. Angiogenesis is involved in the pathogenesis of nonrheumatic aortic valve stenosis. Hum Pathol. 2003; 34:756–763. [PubMed: 14506635]
77. Quinlan AMT, Billiar KL. Investigating the role of substrate stiffness in the persistence of valvular interstitial cell activation. J Biomed Mater Res Part A. 2012; 100A:2474–2482.
78. Hildebrand DK, Wu ZJJ, Mayer JE, Sacks MS. Design and hydrodynamic evaluation of a novel pulsatile bioreactor for biologically active heart valves. Ann Biomed Eng. 2004; 32:1039–1049. [PubMed: 15446500]
79. Ramaswamy S, Gottlieb D, Engelmayr GC, Aikawa E, Schmidt DE, Gaitan-Leon DM, Sales VL, Mayer JE, Sacks MS. The role of organ level conditioning on the promotion of engineered heart valve tissue development in-vitro using mesenchymal stem cells. Biomaterials. 2010; 31:1114–1125. [PubMed: 19944458]

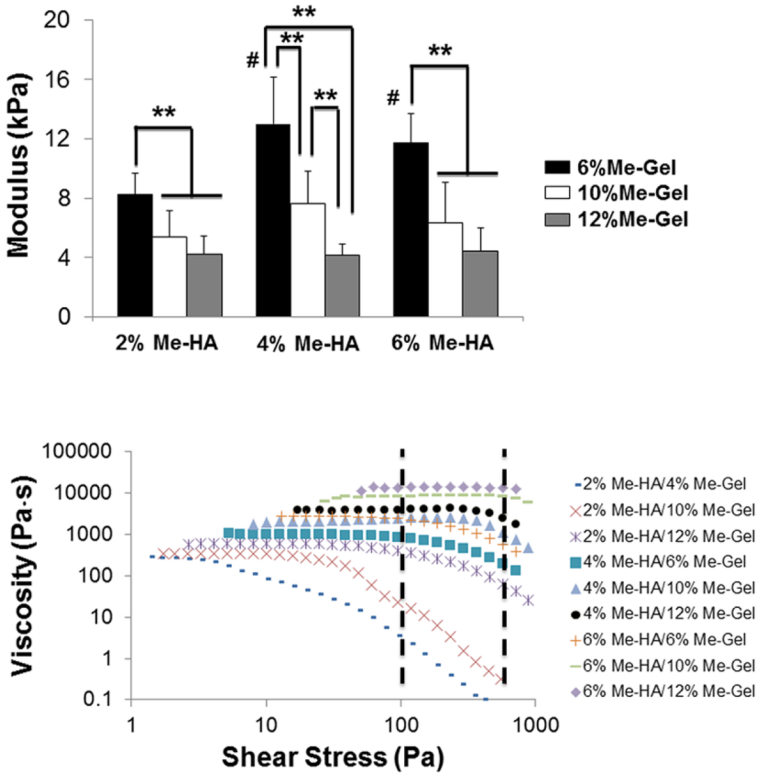

Fig 1.

Tunable mechanical and rheological properties of different hydrogels. (A) Modulus (**p<0.01, # indicated significantly difference between 2%Me-HA/6%Me-Gel and Me-HA (4%, 6%)/6%Me-Gel hydrogels; n=5 for compressive test); (B) viscosity in response to shear stress.

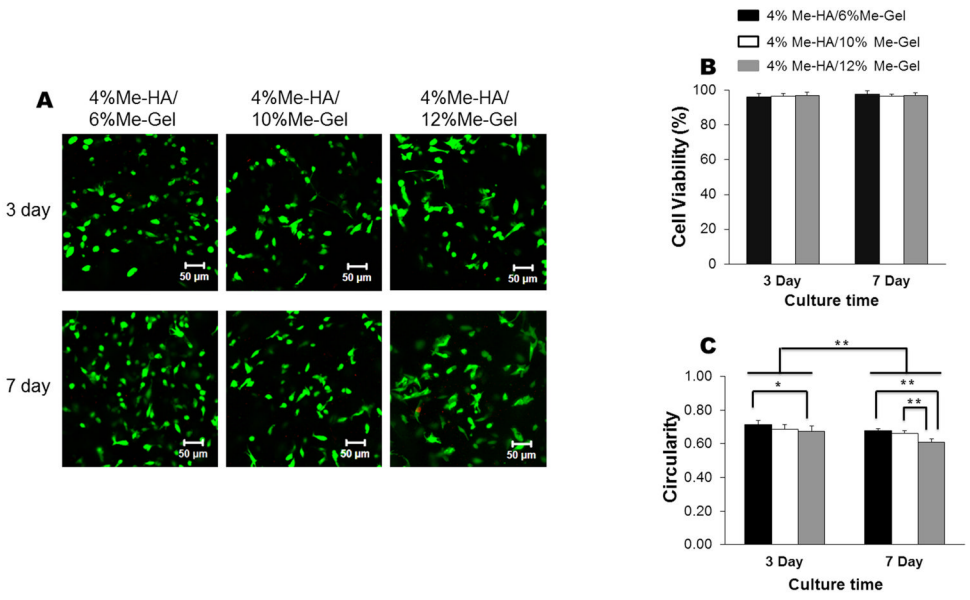

Fig 2.

Live/Dead assay for encapsulated HAVIC within different hydrogels. (A) CLSM images (3 day, up column; 7 day, down column); (B) cell viability measured based on Live/Dead images (n=6); (C) cell circularity measured based on Live/Dead images (*$p < 0.05$, **$p < 0.01$; n=6).

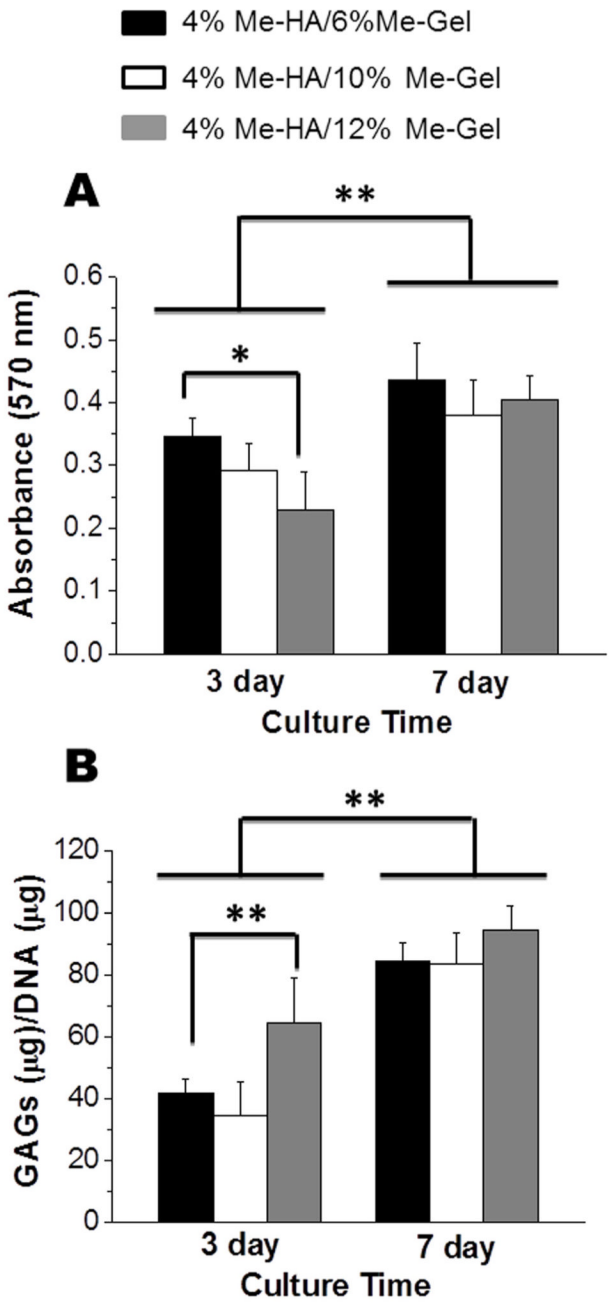

Fig 3.

Encapsulated HAVIC proliferation and GAG deposition within different hydrogels. (A) MTT assay showed the proliferative capacity of HAVIC encapsulated within different hydrogels (*$p < 0.05$, **$p < 0.01$; n=5); (B) GAG content detected by DMMB-based assay and normalized to DNA content (**$p < 0.01$; n=5).

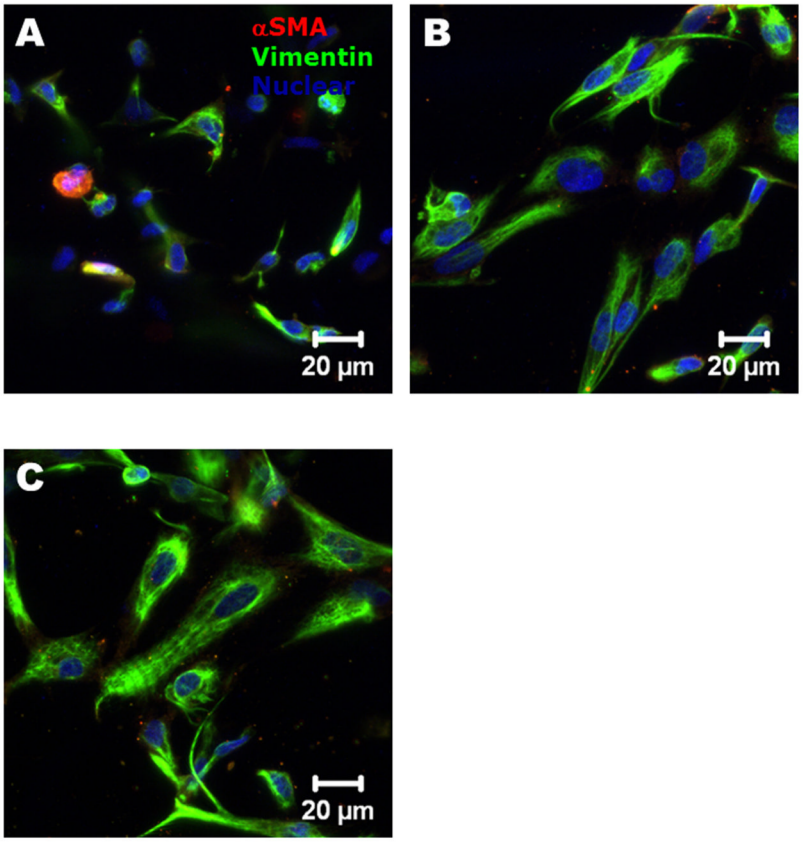

Fig 4.
Immunohistochemical staining for encapsulated HAVIC after 7 day culture. αSMA (red); vimentin (green) and nuclei (blue).

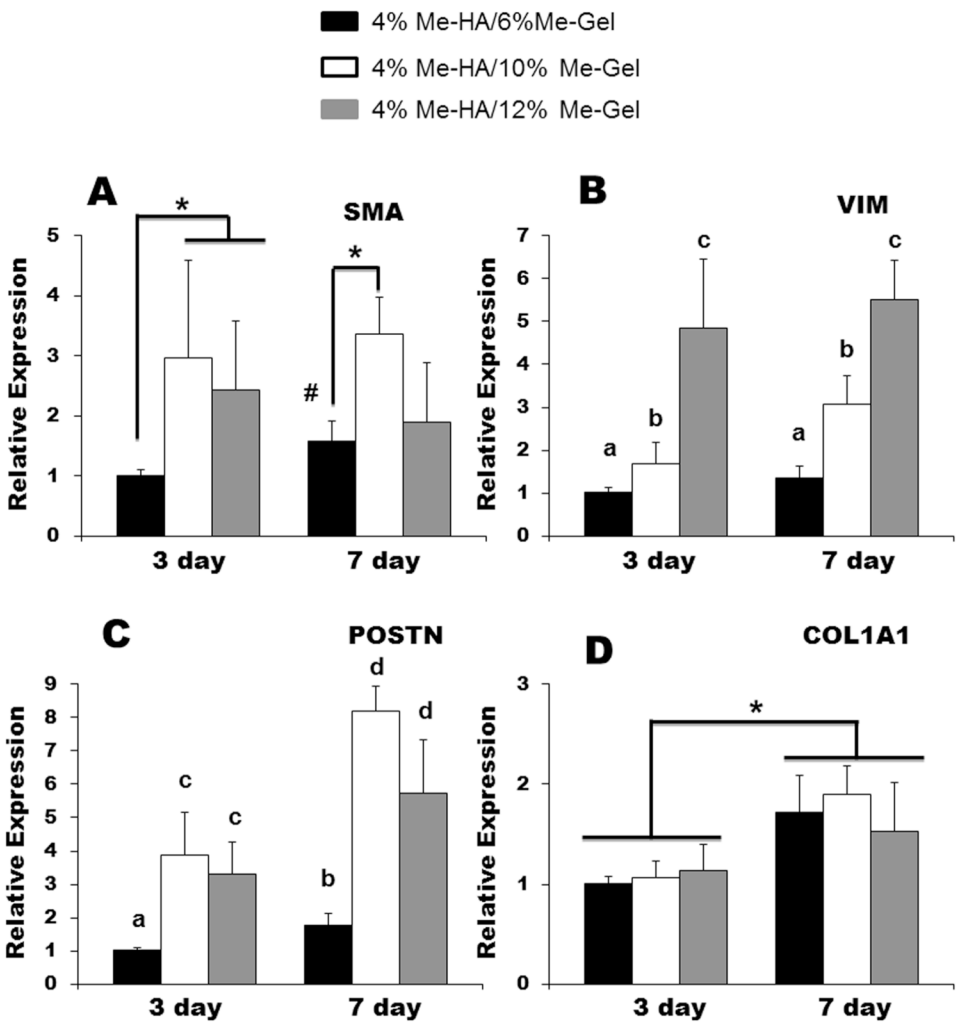

Fig 5.

Real-time PCR analysis of (A) αSMA; (B) vimentin; (C) periostin and (D) collagen 1A1 of HAVIC encapsulated in different hydrogels after 7-day culture. Relative gene expression is presented as normalized to 18S and expressed relative to 4%Me-HA/6%Me-Gel.

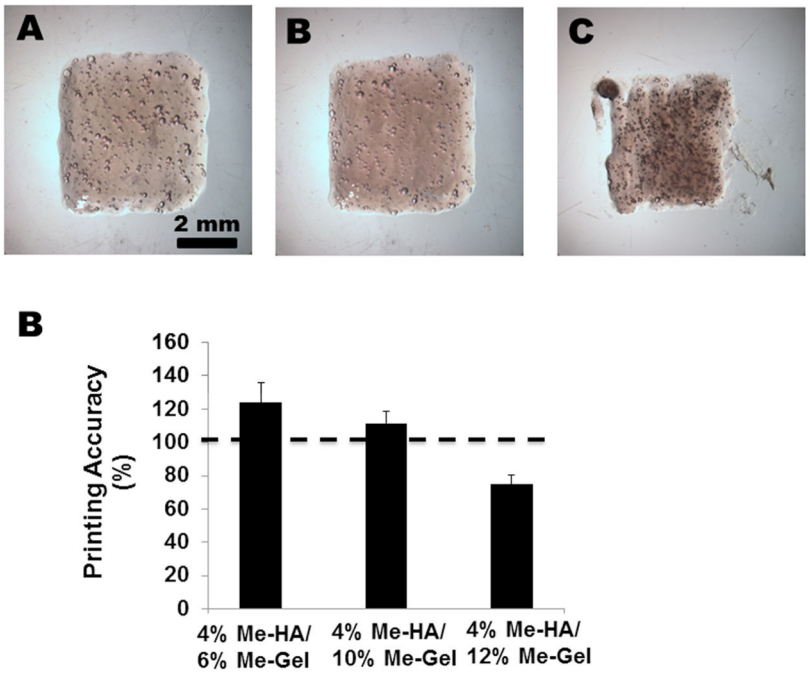

Fig 6.

Bioprinting of cuboid shaped constructs. Representative images of bioprinted constructs using (A) 4%Me-HA/6%Me-Gel, (B) 4%Me-HA/10%Me-Gel and (C) 4%Me-HA/Me-Gel; (D) printed accuracy of bioprinted constructs using different hydrogels (n=5).

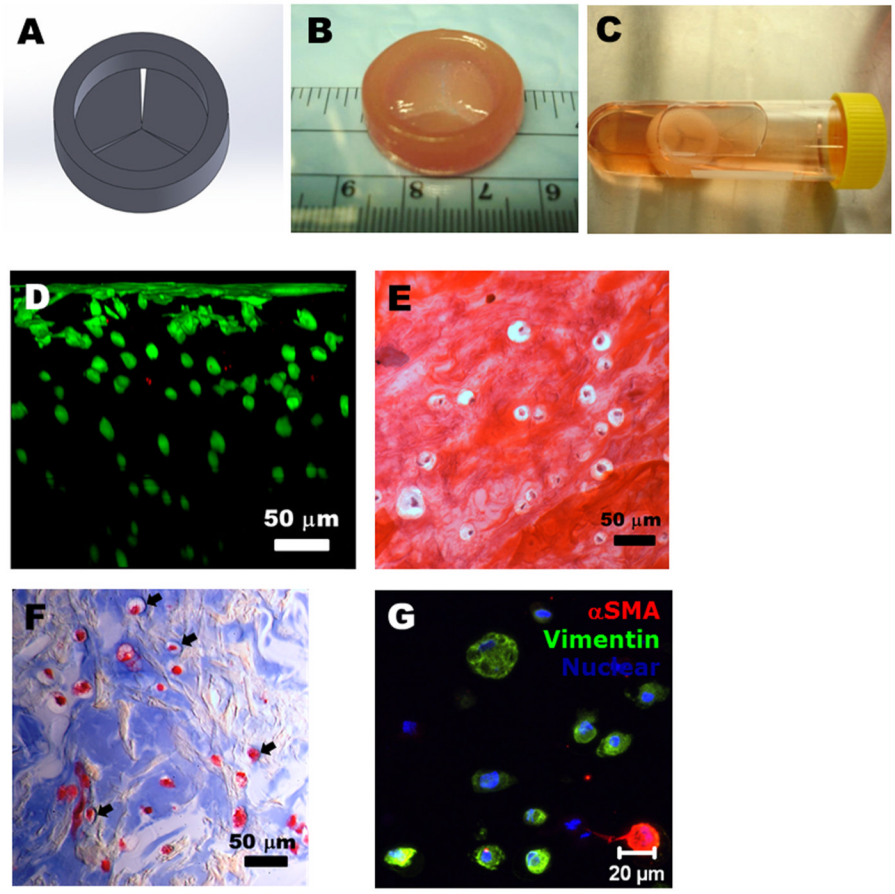

Fig 7.

Bioprinting of heart valve conduit with encapsulation of HAVIC within the leaflets. (A) Heart valve model designed by Solidworks®; (B) as-printed valve conduit; (C) the bioprinted valve conduit kept intact after 7-day static culture in culture tube; (D) cross-sectional view of Live/Dead image showed high cell viability from surface to more than 300 μm depth; (E–F) histological staining of bioprinted leaflets after 7-day culture. (E) Safranin-O staining was used to stain the GAGs red which also stained the Me-HA within the hydrogel red; (F) Masson's Trichrome staining was used to stain collagen blue with also stained the Me-Gel within the hydrogel blue. The arrow showed the newly secreted collagen around the HAVIC, indicating the remodeling process; (G) representative image of immunohistochemical staining for αSMA (green) and vimentin (red), and Draq 5 counterstaining for cell nuclei (blue).